ISSN (Print) 1226-1750
ISSN (Online) 2233-6656
Journal of Magnetics 30(4), 810-815 (2025) https://doi.org/10.4283/JMAG.2025.30.4.810

Development and MRI Safety Evaluation of a Non-Magnetic Pentaprism-Based Visual Aid for Claustrophobia Reduction

Yong-Soo Han[1], Cheol-Soo Park[1*†], and Ho-Beom Lee[2*†]

[1]*Department of Radiological Science, Hallym Polytechnic University, Chuncheon 24210, Republic of Korea*
[2]*Department of Radiology, Wonkwang Health Science University, 514, Iksan-daero, Iksan-si, Republic of Korea*

(Received 6 November 2025, Received in final form 18 December 2025, Accepted 18 December 2025)

Magnetic resonance imaging (MRI) examinations often induce anxiety and claustrophobia in patients, primarily due to the narrow magnet bore (typically 55–65 cm in diameter) and high acoustic noise (65–90 dB). Consequently, approximately 6.5% of scheduled MRI examinations are unable to be completed. While interventions like music therapy or refractive glasses have been explored, few solutions have successfully maintained the patient's direct visual field to enhance comfort and reduce perceptual isolation. This study aimed to design and evaluate a non-ferromagnetic materials, pentaprism-based visual aid that offers stable visual openness during MRI scanning while ensuring full safety and optical clarity. The device was fabricated from polyether-ether-ketone (PEEK) and polymethyl-methacrylate (PMMA) using 3D printing. It incorporates a pentaprism set at 45° that consistently deflects the visual axis by 90° without image inversion, enabling forward vision within the bore. MRI safety was rigorously tested on a 3.0T scanner following the ASTM F2182 (RF heating) and ASTM F2119 (image artifact) standards. The maximum temperature rise (ΔT_{max}) was measured at 0.61 °C (mean $\Delta T = 0.44 \pm 0.09$ °C), remaining well below the 1.0 °C safety threshold. The mean artifact radius r_{art} averaged 1.85 ± 0.5 mm, with signal loss remaining under 7.4% across SE, GRE, and EPI sequences. Furthermore, B_1 homogeneity variation was maintained within 5%, and no image distortion or RF heating was detected in the head coil region. These findings confirm the device's full 3.0T MR Conditional compliance and demonstrate its potential as an effective, non-pharmacological intervention to mitigate MRI-related anxiety through improved visual openness.

Keywords : magnetic resonance imaging (MRI), non-ferromagnetic materials, pentaprism optics, RF-induced heating, image artifact. patient anxiety, claustrophobia

1. Introduction

Magnetic resonance imaging (MRI) is a non-invasive diagnostic technique widely used for the evaluation of neurological, musculoskeletal, and cardiovascular diseases. Despite its superior soft-tissue contrast and the absence of ionizing radiation, many patients experience significant discomfort or anxiety during MRI examinations due to the confined geometry of the magnet bore, high acoustic noise, and restricted visual openness [1, 2]. The cylindrical bore, typically 55-65 cm in diameter, and the intense gradient noise reaching 65-90 dB contribute to a profound sense of spatial restriction and loss of control [2]. Previous clinical reports indicate that approximately 6-7% of scheduled MRI scans are terminated prematurely because of claustrophobia or panic reactions, even in the absence of physical contraindications [3, 4].

To alleviate this psychological distress, various strategies have been explored, including the use of open MRI systems, environmental modifications such as tailored lighting and ventilation, auditory interventions like music therapy, and pharmacological sedation [5, 6]. However, these approaches either necessitate substantial hardware changes (open MRI) or fail to directly address the visual deprivation and loss of spatial orientation experienced by patients within the magnet bore. Inside a conventional head coil, the visual field is largely obstructed by the coil housing, severely limiting the patient's ability to perceive the external space or maintain a sense of openness [7]. This perceptual isolation is strongly associated with

*Corresponding author: Tel: +82-33-240-9353
e-mail: pcs3109@hsc.ac.kr
Tel: +82-63-840-1236, e-mail: feel_love83@hanmail.net
†These authors contributed equally to this work.

heightened anxiety, physiological arousal, and motion artifacts that ultimately compromise image quality.

Recent human-factors studies have emphasized that visual openness and reliable eye-level spatial feedback are critical for maintaining psychological stability under confinement [8, 9]. Devices such as MRI-compatible refractive lenses or mirrors have been proposed to extend the patient's visual field toward external environments, yet these solutions often have inherent limitations. Most commercial prism glasses for MRI are fixed to the head coil or employ bulky mirror assemblies, which can inadvertently exacerbate the feeling of facial enclosure and typically cannot provide personalized visual alignment or refractive correction. Moreover, critical optical performances such as bias accuracy, distortion, and light transmittance are rarely quantitatively validated or reported.

This investigation provides a technical foundation for the future clinical application of visual-field-enhancing devices to mitigate MRI-related anxiety, thereby expanding the concept of human-centered MRI device design that integrates optical engineering with patient comfort.

To address these existing gaps, the present study proposes a novel pentaprism-based, non-magnetic visual aid that allows patients to maintain a stable forward visual field during MRI examinations while fully satisfying stringent safety and imaging compatibility requirements. A pentaprism, unlike a plane mirror system, provides a constant 90° deflection angle that is independent of beam incidence angle and maintains a non-inverted image [10]. This makes it an ideal element for precise visual redirection in confined environments. This optical element is integrated into a compact, eyewear-type device fabricated from non-ferromagnetic, high-performance materials: polyether ether ketone (PEEK) for the frame and polymethyl methacrylate (PMMA) for the prism [11], ensuring both optical clarity and MRI compatibility.

The design of MRI-compatible devices imposes stringent physical and material constraints. All components must be non-conductive, non-ferromagnetic, and dimensionally stable under strong static (B_0) and gradient (dB/dt) fields. Crucially, the device must not introduce RF-induced heating (ΔT <1 °C) or cause significant image artifacts (≤ 5 mm radius) as defined by ASTM F2182 and F2119 [12]. Therefore, the present study was structured with two primary objectives. First, to design and fabricate a 3D-printed, non-magnetic pentaprism visual aid optimized for use inside a standard 3.0T MRI head coil. Second, to evaluate its environmental MRI safety, specifically focusing on RF heating, image artifact size, and B_1 field homogeneity, according to international standards.

2. Materials and Methods

2.1. Device Design and Fabrication

The proposed visual aid device consists of a pentaprism optical module integrated into a lightweight, eyeglass-like

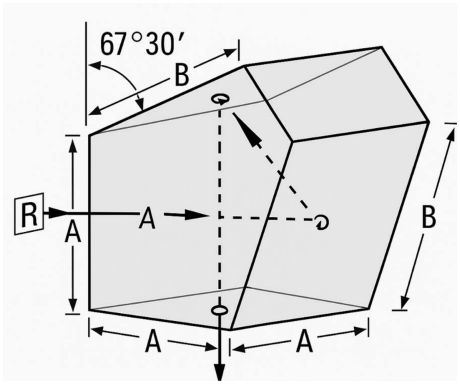

Fig. 1. Geometric configuration and optical path of a pentaprism. The incident beam (R) undergoes two total internal reflections at 45° surfaces, producing a non-inverted output beam deviated by a constant 90°.

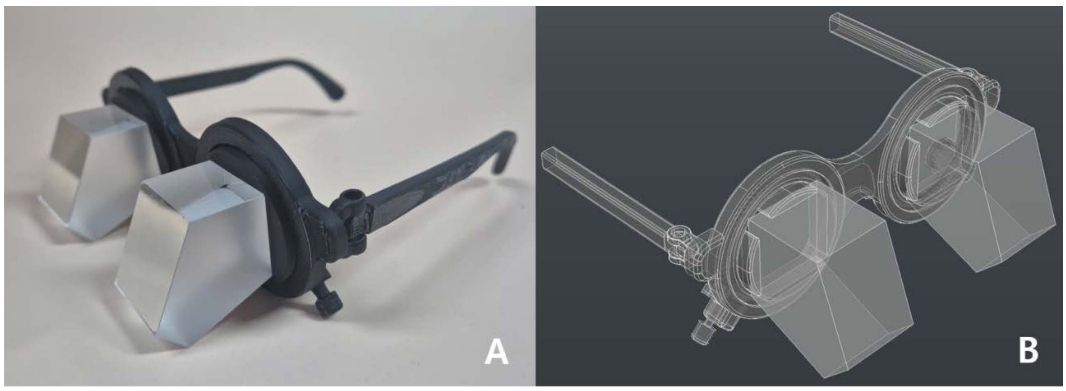

Fig. 2. Illustrates the optical principle and mechanical implementation of the proposed pentaprism visual aid. (A) optical ray-trace diagram of the pentaprism visual aid and (B) CAD 3D rendering.

frame. The optical prism is fabricated from PMMA, which has a refractive index of n = 1.491 at 589 nm. Both reflective surfaces of the prism were coated with an anti-reflection (AR) layer effective across the visible spectrum (range 400-700 nm). The prism geometry is optimized to maintain a constant 90° deflection, ensuring a non-inverted image regardless of subtle head movements (Fig. 1).

The frame was modeled using SolidWorks 2024 and fabricated via selective laser sintering (SLS) using PEEK, a high-strength, non-magnetic thermoplastic polymer (density = 1.31 g/cm³, tensile strength = 90 MPa). Each component, including the frame, prism holder, and nose pad, was securely assembled using non-metallic press-fit joints (Fig. 2). The entire device weighs 78g and features an adjustable interpupillary distance (PD) range (55-70 mm), as well as interchangeable diopter carriers (-6.00D to +6.00D).

2.2. MRI Safety Evaluation

MRI safety was evaluated using a Philips Achieva scanner (B_0 = 3.0T, 32-channel head coil) in accordance with ASTM F2182 (RF heating) and ASTM F2119 (image artifact) standards.

2.2.1. RF heating test

A standard gel phantom (0.5 % NaCl, 1.2 % agar, conductivity = 0.5 S/m) was prepared following ASTM F2182 specifications. The device was fixed to the phantom surface at the "forehead position." Fiber-optic temperature probes (resolution 0.1 °C) were positioned at P1 (temporal frame), P2 (prism housing), P3 (nasal bone), and Pref (reference area) (10 cm away). Scans were performed for 15 minutes at 3.0T, whole-head SAR = 3.2 W/kg. Temperatures were recorded at 1 Hz under the following parameters: Turbo Spin-Echo (TSE), TR/TE = 500/10 ms, flip = 150°, ETL = 8, and slice = 5 mm. Temperature rise (ΔT) was corrected for ambient drift using Pref. Reproducibility was ensured with three repetitions. The safety limit for the test was ΔT <1 °C.

2.2.2. MRI Artifact and B_1 Homogeneity Test

A standard homogeneous phantom (diameter = 180 mm) based on the ASTM F2119 standard was utilized to measure MRI artifacts. This phantom is used to quantitatively assess the magnitude of susceptibility artifacts caused by medical devices. Scans were acquired three times each in the B_0-parallel direction using Spin Echo (SE), Gradient Echo (GRE), and Echo Planar Imaging (EPI) sequences at 3.0T (Table 1). The artifact area was defined as the region of pixels exhibiting a signal loss of 30 % or more compared to the reference image. The maximum artifact radius (r_{art}) was defined as the maximum radius of the signal void measured from the edge of the device. The calculated artifact radius was used to assess the potential invasion of nearby structures of interest in clinical use. The effect of r_{art} was calculated using MATLAB. To assess radiofrequency field homogeneity (ΔB_1rms), B_1 maps were acquired using the vendor's sequence (FA = 60°).

Table 1. Summarizes the acquisition parameters used for the ASTM F2119 artifact assessment at 3.0 T.

Parameter	SE*	GRE*	GRE*	EPI*
TR(ms)	500	100	100	2000
TE(ms)	20	10	25	30
Matrix	256 × 256	256 × 256	256 × 256	256 × 256
FOV	220 × 220	220 × 220	220 × 220	220 × 220
Slice thickness(mm)	5	5	5	5
Bandwidth(Hz/pixel)	200	200	200	320

*SE = Spin Echo, *GRE = Gradient Echo, *EPI = Echo Planner Image

3. Results

3.1. RF Heating Analysis

Under the highest exposure condition (SAR = 3.2 W/kg, 15 min), the maximum temperature rise (ΔT_{max}) was 0.61 °C, recorded at the prism housing (P2). The average ΔT_{peak} across all measurement locations was 0.44 ± 0.09 °C, with a rise rate of 0.03-0.04 °C/min. All measured values were significantly below the ASTM safety limit (ΔT <1 °C) (Table 2). The negligible heating confirms that the PEEK and PMMA components exhibit low dielectric loss and minimal eddy current induction,

Table 2. Reports RF-induced temperature rises measured according to ASTM F2182 under the highest exposure condition (SAR = 3.2 W/kg for 15 min at 3.0 T).

Location	ΔT_peak (°C)*	ΔT_15min (°C)*	dT/dt_initial (°C/min)*
P1 (temporal frame)	0.42 ± 0.05	0.38 ± 0.04	0.03 ± 0.01
P2 (prism housing)	0.55 ± 0.07	0.50 ± 0.06	0.04 ± 0.01
P3 (nasal bone)	0.36 ± 0.03	0.33 ± 0.03	0.03 ± 0.01
Pref (reference area)	0.10 ± 0.02	0.08 ± 0.01	0.01 ± 0.00

*ΔT_peak (°C) = maximum temperature change, *ΔT_15min (°C) = temperature change after 15 minutes, *dT/dt_initial (°C/min) = initial temperature increase rate

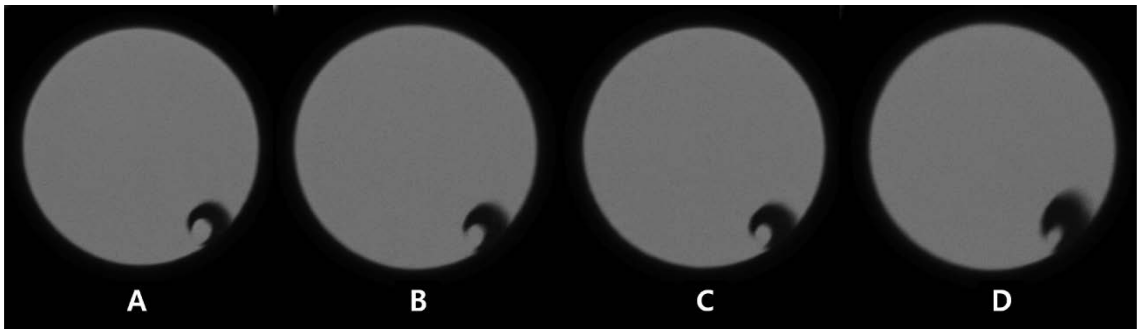

Fig. 3. MRI Artifact Phantom Images by Sequence (3.0T), (A) Spin Echo (SE) TR/TE = 500/20 mm, (B) Gradient Echo (GE) TR/TE = 100/10 mm, (C) Gradient Echo (GE) TR/TE = 100/25 mm, (D) Echo Planner Image (EPI) TR/TE = 2000/30 mm.

Table 3. Summarizes the quantitative MRI artifact characteristics of the pentaprism visual aid according to ASTM F2119 across representative pulse sequences.

Sequence (TR/TE)	Orientation	Max artifact radius* (mm)	Artifact Area (mm²)	Signal intensity reduction (%)
SE (500/20)	Parallel	1.4 ± 0.3	12.6 ± 3.1	4.3 ± 1.0
GRE (100/10)	Parallel	1.8 ± 0.4	15.9 ± 3.4	5.1 ± 1.1
GRE (100/25)	Parallel	2.0 ± 0.5	18.2 ± 3.7	6.2 ± 1.5
EPI (2000/30)	Parallel	2.2 ± 0.6	20.4 ± 4.2	7.4 ± 1.6

(mean ± SD, n = 3)
*Max artifact radius = The furthest distance (mm) affected from the edge of the device

meeting the 3.0T MR Conditional criteria even under high SAR conditions.

3.2. Image Artifact Analysis

Image distortion and signal loss characteristics of the pentaprism glasses were analyzed using the ASTM F2119 method (Fig. 3). Artifact maps obtained from the SE, GRE, and EPI sequences are summarized in Table 3. The average maximum artifact radius (r_{art}) across all sequences was 1.85 ± 0.45 mm, with a maximum individual reading of 2.3 mm observed in the EPI sequence. The average signal attenuation was 5.75 ± 1.30 % (ranging from 4.3-7.4 %). B_1 field analysis revealed a homogeneity variation (ΔB_1rms) of 4.2 ± 1.1 %, which is well within the acceptable 5% tolerance. Subtraction images revealed highly localized signal voids (< 2 mm) only near the prism edges. These data demonstrate that the device induces negligible susceptibility artifacts, consistent with the use of non-metallic components. Minimal signal loss or distortion due to magnetic susceptibility differences was observed, ensuring no impact on the actual head imaging area.

4. Discussion

This study validated the technical feasibility and MRI suitability of a non-magnetic pentaprism-based visual aid specifically designed to improve the field of view during MRI examinations. The device showed excellent optical precision, with a deflection accuracy of 90.02° ± 0.06°, MTF = 0.43 @ 10 lp/mm, transmittance = 91 %, and geometric distortion = 1.1 %. Measurements using ASTM F2182 and F2119 test standards demonstrated minimal RF induction heating (ΔT_{peak} = 0.61 °C at 3.0T, SAR = 3.2 W/kg), limited magnetic susceptibility artifact ($r_{art} \leq 2$ mm), and excellent B_1 uniformity ($\Delta B_{1rms} < 5$ %). Overall, these results confirm that the combination of PEEK and PMMA in a fixed 45° pentaprism configuration offers both high optical performance potential and MRI safety compliance.

The use of a pentaprism is a core advantage. Unlike flat mirrors, which require precise, stable alignment for consistent deflection, pentaprisms inherently guarantee a fixed 90° beam deflection independent of the angle of incidence [10]. This property is crucial as it ensures consistent image orientation without inversion, which is highly beneficial for precise visual redirection in the dynamic, confined environment of an MRI bore.

This is especially important in MRI, where patient positioning within a narrow bore limits the view, and slight head movements are common. Mirror-based solutions, including those used in some commercial MRI

eyewear, typically suffer from image inversion, potential field distortion, and alignment drift with repeated use or subtle mechanical vibrations [9]. These drawbacks not only degrade optical fidelity but can also contribute to psychological discomfort due to a distorted or inverted perceived environment.

The current pentaprism design provides a geometrically stable, non-inverted forward field of view that mimics the visual openness of single-aperture scanners without requiring major changes to the MRI system hardware [13]. Furthermore, the 3D-printed PEEK housing, a high-performance polymer, has a magnetic susceptibility nearly identical to that of human tissue, rendering magnetic field disturbance negligible [14]. Consistent with this, no measurable B_0 distortion was detected beyond 2 mm from the device, and the maximum artifact size remained below 2.3 mm even during the highly susceptible GRE and EPI sequences (Table 3). This study experimentally confirmed these material advantages.

RF heating remains a critical safety parameter. ASTM F2182 defines ΔT of less than 1.0 °C under 3 W/kg SAR exposure as negligible for MR Conditional labeling. The device recorded an average ΔT_{peak} of 0.44 ± 0.09 °C, well below this threshold, confirming minimal electromagnetic coupling with the scanner's RF field. This result is consistent with findings that non-conductive, polymer-based materials are optimal for mitigating eddy current-induced heating [14, 15]. Moreover, the B_1 mapping results showed a uniformity deviation of only 4.2 ± 1.1 %, demonstrating that the pentaprism and frame structure did not induce local RF shadowing or significant RF absorption effects [15]. Lee *et al.* [16] demonstrated that a fixed-geometry prism offers superior signal stability compared to systems with long dielectric paths (e.g., fiber optics or complex mirror assemblies) that can act as an antenna or disrupt the transmitted electromagnetic field.

From a patient perspective, visual openness has a measurable impact on anxiety. Enders *et al.* [17] demonstrated that open-bore or single-aperture MRI systems significantly reduced claustrophobia compared to conventional closed scanners, resulting in nearly 15% higher exam completion rates. However, open systems often suffer from poor signal-to-noise ratio (SNR). Optimized accessories can directly impact scanner efficiency by minimizing patient repositioning and reexaminations due to anxiety-related motion artifacts [12].

The integration of the pentaprism device requires no mechanical adjustment of the head coil and allows for installation and removal in under a minute, meeting important operational criteria. Furthermore, the 3D-printed modular frame allows for rapid customization of interpupillary distance and facial curvature, ensuring a consistent fit across a wide range of patient anatomy. These ergonomic considerations align with the broader trend in MRI accessory development toward "patient-centered engineering," which combines safety, comfort, and workflow efficiency.

While this study provides comprehensive technical validation, several limitations should be acknowledged. First, the evaluation was conducted using standardized phantom equipment rather than human subjects; thus, patient movement, eye tracking, and subjective anxiety measurements were not included. Second, artifact quantification relied solely on 2D cross-sectional analysis as per ASTM F2119. Future studies should expand this to volumetric 3D artifact mapping to enable more detailed susceptibility profiling. Third, durability under repeated sterilization and long-term material aging remains to be investigated.

Despite these limitations, the results establish a firm foundation for clinical translation. The consistent performance across SE, GRE, and EPI sequences indicates that the pentaprism visual aid can be safely used in most diagnostic MRI protocols. Future patient studies should integrate psychometric tools such as the GAD-7 scale to objectively quantify anxiety reduction. Verified evidence would strongly support the use of such optical devices as non-pharmacological interventions for claustrophobia mitigation in MRI.

5. Conclusion

In this study, we successfully developed and evaluated a non-magnetic pentaprism-based visual aid designed to enhance visual clarity and patient comfort during MRI examinations. This device, combining a 45° PMMA pentaprism with a 3D-printed PEEK frame, achieved high optical fidelity and satisfied all 3.0T MRI compatibility and safety standards (ASTM F2182 and F2119). The maximum temperature rise 0.61 °C (ΔT < 1 °C), and the maximum artifact radius was 2.3 mm (r_{art} < 5 mm). Future work will focus on evaluating its clinical efficacy through in vivo anxiolytic studies and validation in high-field environments. Overall, this study demonstrates how human-centered, MR-safe optical devices can enhance imaging efficiency and the overall patient experience, creating a safer, more comfortable, and technologically advanced MRI environment.

Acknowledgments

This research was supported by Hallym Polytechnic

University.

References

[1] H. B. Lee and Y. S. Han, J. Magn. **30**, 434 (2025).
[2] M. Dewey, J. Schink, and A. Hamm, Eur. Radiol. **24**, 2325 (2014).
[3] J. Enders, M. Zimmermann, P. Rief, and M. Dewey, BMC Med. Imaging **11**, 12 (2011).
[4] E. Scappatura, F. Rossi, and G. Leone, Front. Psychol.: Health **13**, 1182 (2024).
[5] S. Jain, R. Patel, and H. Mehta, Eur. J. Radiol. **168**, 111238 (2025).
[6] S. Pritchard and D. Evans, Radiogr. **28**, 102 (2022).
[7] R. Al-Nassar, L. Ahmed, and K. Hasan, BMC Med. Imaging **22**, 55 (2022).
[8] T. Blair, C. Richardson, and P. Martin, Front. Neurosci. **19**, 512 (2025).
[9] Magmedix Inc., MRI Prism Glasses: Prduct Specification Sheet, Technical Document, Magmedix Inc. (2025).
[10] MOK Optics, Optical Prism Systems: Technical Whitepaper, Report No. MOK-OPS-2023-01 (2023).
[11] J. W. Huh, S. J. Lee, and T. Kim, IEEE Trans. Med. Imaging **42**, 1850 (2023).
[12] A. Müller, R. Schmidt, and M. Reimann, Magn. Reson. Mater. Phys. Biol. Med. (MAGMA) **36**, 1127 (2023).
[13] B. C. Lee, J. H. Lim, and Y. S. Kwon, iMRI **25**, 305 (2021).
[14] MRI Med, The Science Behind Non-Ferromagnetic Medical Devices, Technical Report, MRI Med (2022) p. 17.
[15] AliMed Inc., MRI Accessories: Improving Safety and Efficiency, Product Whitepaper, AliMed Inc. (2023) p. 8.
[16] H. Lee and S. Park, iMRI **25**, 233 (2021).
[17] J. Enders, M. Zimmermann, P. Rief, and M. Dewey, PLoS One **6**, e24235 (2011).